Journal of Computational Physics 452 (2022) 110910

Contents lists available at ScienceDirect

Journal of Computational Physics

www.elsevier.com/locate/jcp

A recycling preconditioning method with auxiliary tip subspace for elastic crack propagation simulation using XFEM

Xingding Chen [a], Xiao-Chuan Cai [b,*]

[a] School of Mathematics and Statistics, Beijing Technology and Business University, Beijing 100048, PR China
[b] Department of Mathematics, University of Macau, Macau, PR China

ARTICLE INFO

Article history:
Received 28 July 2021
Received in revised form 16 December 2021
Accepted 19 December 2021
Available online 29 December 2021

Keywords:
Extended finite element method
Domain decomposition preconditioners
Sequence of linear systems
Crack propagation
Auxiliary tip subspace

ABSTRACT

In this paper, we propose a recycling preconditioning method with auxiliary tip subspace for solving a sequence of highly ill-conditioned linear systems of equations of different sizes arising from elastic crack propagation problems discretized by the extended finite element method. To construct a Schwarz type preconditioner, the finite element mesh is decomposed into crack tip subdomains, which contain all the degrees of freedom (DOFs) of the branch enrichment functions, and regular subdomains, which contain the standard DOFs and the DOFs of the Heaviside and the Junction enrichment functions. As cracks propagate these subdomains are modified accordingly, and the subdomain matrices are constructed as the restriction of the global matrix to the subdomains. In the overlapping Schwarz preconditioners, the crack tip subproblems are solved exactly and the regular subproblems are solved by some inexact solvers, such as ILU. We consider problems with and without crack intersections and develop a simple scheme to update, instead of re-computing, the subdomain problems as cracks propagate, in which only crack tip subdomains are updated around the new crack tips and all the regular subdomains remain unchanged. Therefore, no extra search is required, and the sizes of crack tip subproblems do not increase as cracks propagate, which greatly saves the computational cost. Moreover, starting from the second system, the Krylov subspace method uses a nontrivial initial guess constructed using the solution of the previous system with a modification around the new crack tips. The strategy accelerates the convergence remarkably. Numerical experiments demonstrate the efficiency of the proposed algorithms applied to problems with several types of cracks.

1. Introduction

The extended finite element method (XFEM) [1,2,12] is a powerful technique for solving fracture problems with discontinuities, singularities and localized deformations. When modeling cracks with the standard finite element method (FEM), one often requires special meshes whose element edges coincide with the crack surface and nodes be placed on each side of the crack to allow material separations along the crack line. Moreover, the mesh refinement is often needed in order to simulate crack propagations, that may significantly increase the complexity of the topologies and the computational cost each time new cracks generate. The key idea of XFEM is that the mesh is independent of the crack geometry, which means

* Corresponding author.
E-mail addresses: chenxd@th.btbu.edu.cn (X. Chen), xccai@um.edu.mo (X.-C. Cai).

https://doi.org/10.1016/j.jcp.2021.110910
0021-9991/

that structured meshes can be adopted to resolve the crack problems. The discontinuities along the crack interfaces and singularities near crack tips are captured through some additional enrichment functions, which satisfy a partition of unity. Therefore, special elements or mesh refinements are not required in XFEM.

A major drawback of XFEM is that the linear system arising from such discretization is very ill-conditioned and requires robust iterative solvers, see [3]. For example, consider the linear elasticity problem, the condition number of the stiffness matrix in XFEM is $O(h^{-4})$ (h is the mesh size), even if a single, non-polynomial enrichment function is used, while the condition number of the stiffness matrix in FEM is only $O(h^{-2})$. One way to reduce the condition number is to modify the enrichment functions, such as the stable generalized finite element methods [3,5,15,21,22] and the improved XFEM [18,20]. The other way to reduce the condition number of XFEM is through preconditioning, which is the main focus of this paper. As cracks grow, multiple linear systems of different sizes need to be solved. In stead of recompute, we introduce some strategies to reuse certain information from solving the previous system.

Among the well-known preconditioners leading to fast convergence are the multigrid methods and domain decomposition methods (DDM)). There are two types of XFEM, namely topological XFEM and geometric XFEM. For topological XFEM, there are several preconditioning techniques. In [13], a DDM is employed, and the condition number of the preconditioned system is close to that of FEM without any enrichments. In [8], a simple and efficient preconditioner is proposed for XFEM involving only the Heaviside enrichment function. A smoothed aggregation algebraic multigrid (AMG) preconditioner is studied in [16] and an adaptive domain decomposition preconditioner is studied in [19], respectively. In [4], a multiplicative Schwarz domain decomposition preconditioner is proposed, where the physical domain is decomposed into cracked subdomains and healthy subdomains. The cracked subproblems, which contain both the DOFs of the Heaviside enrichment function and the branch enrichment functions, are solved exactly. The healthy subproblems, which contain only the standard DOFs, are solved approximately by one AMG V-cycle. This domain decomposition approach is extended to multiple propagating cracks in [29], in which two adaptive search algorithms are developed to update the subdomains. One is the level set update scheme and the other is the neighbor search scheme. No matter which search algorithm is adopted, the size of cracked subproblems become larger and larger, and this increases the computational cost considerably. Note that the cases of crack intersections, which are more complex and difficult but more important for realistic applications, are not considered in [29]. For geometric XFEM, we introduced some effective one- and two-level domain decomposition preconditioners for stationary elastic crack problems in [30], in which we discovered that the main contributor to the large condition number is the crack tip, not the crack line. The physical domain is decomposed into the crack tip subdomain, which contains all the DOFs of the branch enrichment functions, and the regular subdomains, which contain the standard DOFs and the DOFs of the Heaviside enrichment function. In the one-level additive Schwarz and restricted additive Schwarz preconditioners, the crack tip subproblem is solved directly and the regular subproblems are solved by some inexact solvers, such as ILU. Moreover, an unconventional coarse problem is proposed to accelerate the convergence in the two-level method. As an extension of [30], in the present paper, we construct a recycling preconditioning method with auxiliary tip subspace for crack propagation problems modeled by the geometric XFEM, in which different types of crack intersections are considered.

The outline of this paper is as follows. As cracks develop, a new system of algebraic equations needs to be constructed and solved. However, existing recycling Krylov subspace algorithms [28] for solving a sequence of systems can't be used since the systems all have different sizes. We introduce a strategy based on the auxiliary tip subspace to start the iteration using a modified solution from the previous system (i.e., previous crack) when solving a new system corresponding to the new crack and numerical experiments show that this approach is quite efficient. The XFEM discretization for a model problem is explained in Section 2, including a description of crack intersection. In Section 3, we focus on the crack propagation. In Section 4, some domain decomposition techniques are discussed for solving algebraic systems arising from crack propagation problems. Some effective Schwarz preconditioners and a new way to construct the initial guess for GREMS is introduced and studied. Numerical experiments are shown in Section 5, followed by some concluding remarks in Section 6.

2. XFEM for elastic crack propagation problems

In this section, we first give a description of the governing equations for elasto-statics and their associated weak form. Then, we consider situations when cracks are disjoint or intersecting.

2.1. A model problem without crack intersection

Consider the domain $\Omega \subset \mathcal{R}^2$ with the boundary $\Gamma = \Gamma_u \cup \Gamma_t$. We assume a prescribed displacement is imposed on Γ_u and a Neumann boundary condition is imposed on Γ_t. The crack line Γ_c is traction-free, p^+ is the crack pressure above the crack line, p^- is the crack pressure below the crack line, as shown in Fig. 1. The equilibrium equations and boundary conditions are given as

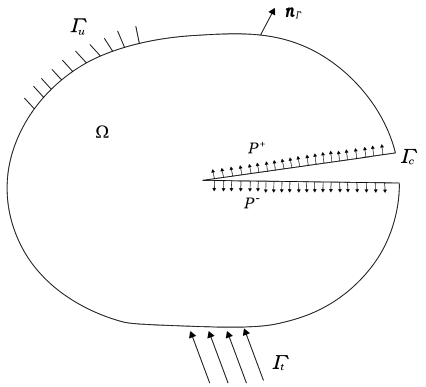

Fig. 1. A two-dimensional domain subjecting to loads and with a crack.

$$\begin{cases} \nabla \cdot \sigma + \mathbf{b} = 0 \ \text{ in } \Omega, \\ \mathbf{u} = \bar{\mathbf{u}} \ \text{ on } \Gamma_u, \\ \sigma \cdot \mathbf{n} = \mathbf{t} \ \text{ on } \Gamma_t, \\ \sigma \cdot \mathbf{n} = 0 \ \text{ on } \Gamma_c^+, \\ \sigma \cdot \mathbf{n} = 0 \ \text{ on } \Gamma_c^-, \end{cases} \tag{1}$$

where $\mathbf{u}$ is the displacement, $\bar{\mathbf{u}}$ is the fixed boundary displacement, $\mathbf{n}$ is the unit outward normal, Γ_c^+ is the upper crack line, Γ_c^- is the lower crack line, σ is the Cauchy stress, and $\mathbf{b}$ is the body force per unit volume.

We assume that the strain and the displacement are small, therefore the kinematical equations consist of the strain-displacement relation

$$\varepsilon = \varepsilon(\mathbf{u}) = \nabla_s \mathbf{u},$$

where ∇_s is the symmetric part of the gradient operator, and the constitutive relation is given by the Hooke's law

$$\sigma = C : \varepsilon,$$

where C is the Hooke tensor.

The space of admissible displacement fields is defined by

$$\mathcal{U} = \{\mathbf{v} \in \mathcal{V} : \mathbf{v} = \bar{\mathbf{u}} \text{ on } \Gamma_u, \ \mathbf{v} \text{ is discontinuous on } \Gamma_c\},$$

where the space $\mathcal{V}$ is related to the regularity of the solution. A detailed description for the domain with an internal boundary can be found in [14]. We note that the space $\mathcal{V}$ allows for discontinuous functions across the crack line. The test function space is defined similarly as

$$\mathcal{U}_0 = \{\mathbf{v} \in \mathcal{V} : \mathbf{v} = 0 \text{ on } \Gamma_u, \ \mathbf{v} \text{ is discontinuous on } \Gamma_c\}.$$

The weak form of the equilibrium equations (1) is to find $\mathbf{u} \in \mathcal{U}$ such that

$$\int_\Omega \varepsilon(\mathbf{u}) : C : \varepsilon(\mathbf{v}) d\Omega = \int_\Omega \mathbf{b} \cdot \mathbf{v} d\Omega + \int_{\Gamma_t} t \cdot \mathbf{u} ds + \int_{\Gamma_c} p \cdot w ds, \quad \forall \mathbf{v} \in \mathcal{U}_0, \tag{2}$$

where the crack pressure $p = p^+ = -p^-$, the crack width $w = u^+ - u^-$, u^+ denotes the displacement above the crack line and u^- denotes the displacement below the crack line. It is shown in Belytschko and Black [1] that the above weak form is equivalent to the strong form (1), including the traction-free condition on the crack line.

To discretize (2), we apply XFEM which uses level set functions to detect the locations of the nodes around the crack and its tips. There are two types of typical enrichment functions, see [1,12].

Heaviside enrichment function: all the nodes along the crack line, excluding those at the tips, are enriched by the Heaviside function to incorporate a strong discontinuity

$$H(x) = \begin{cases} -1 & \text{above the crack line,} \\ 1 & \text{below the crack line.} \end{cases} \tag{3}$$

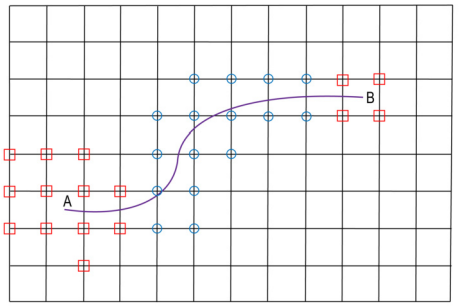

Fig. 2. Crack located on a structured mesh. Blue circled nodes are enriched with the Heaviside function while red squared nodes are enriched by branch functions. (For interpretation of the colors in the figure(s), the reader is referred to the web version of this article.)

Branch enrichment functions: nodes of the elements containing or near crack tips are enriched with a set of four functions, that model the near-tip analytical solution by incorporating the tip singularities; i.e., for $l = 1, \cdots, 4$,

$$F_l(r(x), \theta(x)) = \left\{ \sqrt{r}sin\left(\frac{\theta}{2}\right), \sqrt{r}cos\left(\frac{\theta}{2}\right), \sqrt{r}sin\left(\frac{\theta}{2}\right)sin\theta, \sqrt{r}cos\left(\frac{\theta}{2}\right)sin\theta \right\}, \tag{4}$$

where $(r(x), \theta(x))$ is a polar coordinate system centered at the crack tip x.

It is known that the above four branch enrichment functions (4) are ideal for the linear elastic fracture problems of a straight crack, but the use of them results in a very singular coefficient matrix. There are some remedies to avoid the singularity, such as reduce the set of branch enrichment functions. Since the first function $\sqrt{r}sin\left(\frac{\theta}{2}\right)$ is discontinuous, it can not be omitted. The authors in [26] studied many possibilities, and find that the drop of the fourth function $\sqrt{r}cos\left(\frac{\theta}{2}\right)sin\theta$ does not influence the computational accuracy. Moreover, dropping the fourth function leads to a significant improvement on the number of iterations and the computational time. Therefore, in the rest of the paper we only use three of the functions in (4).

The general expression of the XFEM solution is then written as

$$u^h(x) = \sum_{i \in I} u_i \varphi_i(x) + \sum_{j \in S_H} b_j \varphi_j H(x) + \sum_{k \in S_C} \varphi_k \left(\sum_{l=1}^{3} c_k^l F_l(x) \right), \tag{5}$$

where $\{\varphi_i\}$ are the standard finite element shape functions associated with the degrees of freedom u_i. b_j and c_k^l are the degrees of freedom associated with the enriched nodes, I is the set of nodes, S_H is the set of nodes enriched with the Heaviside function along the crack line, and S_C is the set of nodes enriched with the branch functions. The enrichment strategy is illustrated in Fig. 2.

Two types of tip enrichments are shown in Fig. 2. At the crack tip "B", only the nodes of the element containing the crack tip are enriched with the branch functions, and this method is commonly referred to as the topological XFEM. At the crack tip "A", the nodes of several elements containing or near the crack tip are enriched, and this method is referred to as the geometric XFEM. As is known, the accuracy of the geometric XFEM is satisfactory, but the condition number is much larger than that of the topological FEM, see [15]. In this paper, we focus on preconditioning techniques for the geometric XFEM, which is much more difficult than that of the topological XFEM.

It is known [2] that the order of accuracy of the geometric XFEM is $O(h)$, where h is the mesh size. The condition number of the stiffness matrix is $O(h^{-4})$; see [1,3,12] for details.

2.2. A crack intersection problem

In this section, we describe a XFEM for the crack intersection problem. In Fig. 3, we mark the nodes of an element containing the intersection of two crack lines, and the element is enriched by a Junction enrichment function $J(x)$ to incorporate the strong discontinuity. We use ± 1 to indicate the location of the Junction enriched nodes. Three different elements involving the intersection of two cracks as shown in Fig. 4. Fig. 4(a) shows a second crack joins the main crack, in this case the Junction function in different regions are defined as

$$J_A = 1, \quad J_B = 1, \quad J_C = -1. \tag{6}$$

Fig. 4(b) shows a second crack that is generated from the main crack, in this case the Junction function in different regions are defined as

$$J_A = 1, \quad J_B = -1, \quad J_C = 1. \tag{7}$$

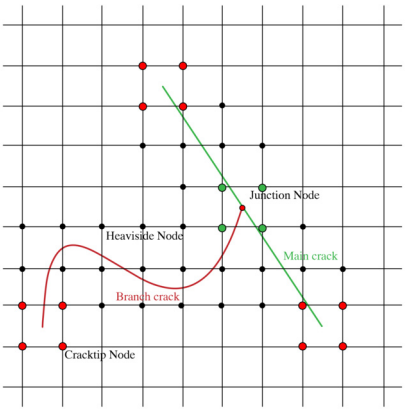

Fig. 3. The schematic diagram of a crack intersection. The green line denotes the main crack, the red line denotes the branch crack. The black nodes are enriched by the Heaviside function, the red nodes are enriched by branch functions, and the green nodes are enriched by the Junction function.

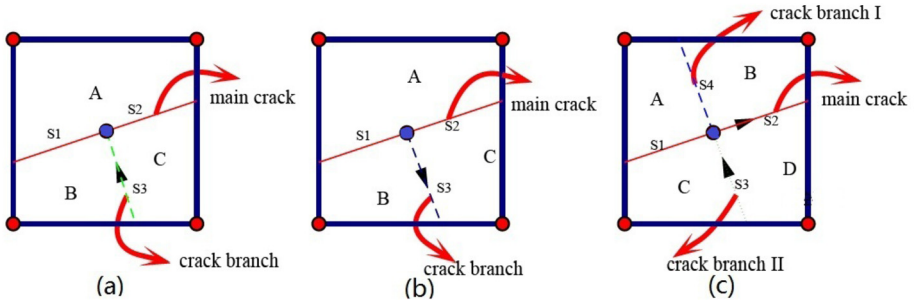

Fig. 4. Different types of crack intersections. The red line denotes the main crack, the green/blue lines denote the branch cracks. The blue node inside the element is the crack intersecting point, and the red vertices are enriched by the Junction function.

Fig. 4(c) shows two cracks crossing each other, in this case the Junction function in different regions are defined as

$$\begin{aligned} &J_A^{branch\ I}=1,\quad J_B^{branch\ I}=-1,\quad J_C^{branch\ I}=-1,\quad J_D^{branch\ I}=-1,\\ &J_A^{branch\ II}=1,\quad J_B^{branch\ II}=1,\quad J_C^{branch\ II}=1,\quad J_D^{branch\ II}=-1. \end{aligned} \tag{8}$$

Then, the interpolation function of the displacement $u^h(x)$, restricting to the elements in Fig. 4(a) and (b), can be written as

$$u^h(x)=\sum_{i=1}^{4}u_i\varphi_i(x)+\sum_{j=1}^{4}\varphi_j(x)H(x)q_j^I+\sum_{k=1}^{4}\varphi_k(x)J(x)q_k^{II}, \tag{9}$$

where q_j^I, q_k^{II} denote the degrees of freedom associated with the Heaviside enriched node and the Junction enriched nodes, respectively. $J(x)$ is defined in (6) and (7).

The interpolation function of the displacement $u^h(x)$, restricting to the element in Fig. 4(c), can be written as

$$u^h(x)=\sum_{i=1}^{4}u_i\varphi_i(x)+\sum_{j=1}^{4}\varphi_j(x)H(x)q_j^I+\sum_{k=1}^{4}\varphi_k(x)J^1(x)c_k^1+\sum_{k=1}^{4}\varphi_k(x)J^2(x)c_k^2, \tag{10}$$

where q_j^I denotes DOFs associated with the Heaviside enriched nodes. c_k^1, c_k^2 denote the DOFs associated with the Junction enriched nodes related to the branch crack I and the branch crack II, respectively. $J(x)$ is defined in (8).

3. Crack propagation

In classical fracture mechanics, the crack propagation is usually determined by three steps, and each step may be obtained with different techniques or criterions. In this paper we choose one of the popular methods.

- Step 1: Computation of the stress intensity factors (or strain energy release rates), e.g., by the J-integral method.
  We utilize a variant of the J-integral method, known as the interaction integral, to extract the mixed-mode SIFs (Stress Intensity Factors). The interaction integral I is defined as

$$I = \int_{\Gamma} q_i P_{ij}^{aux} n_j d\Gamma - \int_{\Omega} q_{i,j} P_{ij}^{aux} d\Omega - \int_{\Omega} q_i P_{ij,j}^{aux} d\Omega,$$

  with

$$P_{ij}^{aux} = \frac{1}{2}\sigma_{kl}\varepsilon_{kl}^{aux}\delta_{ij} + \frac{1}{2}\sigma_{kl}^{aux}\varepsilon_{kl}\delta_{ij} - \sigma_{kj}^{aux}u_{k,i} - \sigma_{kj}u_{k,i}^{aux},$$

  where u^{aux}, ε^{aux} and σ^{aux} are auxiliary displacements, strains and stresses computed from analytical solutions of linear elastic fracture mechanics. See [25,27] for the details.
- Step 2: Verification of the crack stability (whether the crack will propagate or not), determined by the fracture toughness or fracture energy criterions.
  The stability criteria is written as

$$\begin{cases} G < G_c, & \text{crack is stable(will not propagate)}, \\ G \geq G_c, & \text{crack is unstable(will propagate)}, \end{cases}$$

  where G_c is the critical energy release rate of materials, and G is the Strain Energy Release Rates (SERR) computed from the finite element analysis. Note that G can be conveniently expressed as a function of the SIFs as follows

$$G = \frac{1+\nu^2}{E}(K_I^2 + K_{II}^2),$$

  where ν is the Poisson's ratio, E is the Young's modulus. K_I, K_{II} denote the SIFs of mode I and mode II, respectively. Hence, the computation of SIFs at step 1 is also used to determine the SEER which governs the stability of cracks.
- Step 3: Computation of the direction of the crack propagation, e.g., based on the maximum circumferential (hoop) stress criterion.
  In this work, we employ the classical theory of Erdogan and Sih [23] for isotropic materials to determine the angle of the crack propagation. The expression for the angle by which the crack kinks is

$$\theta_c = 2arctan\left(\frac{1}{4}\left[\frac{K_I}{K_{II}} + \sqrt{\left(\frac{K_I}{K_{II}}\right)^2 + 8}\right]\right).$$

  We refer to [24] for more details.

To simulate the crack propagation, we start from a problem with a static crack and denote the corresponding linear system of equations as $A^0u^0 = b^0$ where A^0 is an $n_0 \times n_0$ matrix, u^0 consists of the regular DOF and the enriched DOF, and b^0 is the right-hand side. Based on u^0, and Steps 1-3, a new crack line is computed and the corresponding displacement u^1 is obtained by solving a new linear system of equations $A^1u^1 = b^1$ where A^1 is an $n_1 \times n_1$ matrix. Here n^1 is larger than n^0 when the crack grows, but n^1 is not too much larger than n^0 since the crack grows by at most one grid point at a time. As the crack continues to grow, we construct and solve a sequence of linear system of equations

$$A^k u^k = b^k, \quad k = 0, 1, \ldots \tag{11}$$

As we know, the recycling Krylov subspace methods are very efficient to solve a sequence of linear systems. In [28], a method based on cohesive elements is used to solve some crack propagation problems, in which the size of the global stiffness matrix remains the same in each propagation step. Therefore, the recycling GMRES solver, GCRO-DR, can be used to solve the linear systems. However, in the present paper, since the enriched functions are used to simulate cracks, the size of the global stiffness matrix A^k increases in (11) as cracks propagate, as a result, the recycling GMRES approach can not be applied. In [13], a robust preconditioning technique, which uses several Cholesky decompositions and a LQ decomposition of the global stiffness matrices, is adopted in the MINRES iterative solver. In [29], a domain decomposition algorithm is proposed, in which an inexact multiplicative Schwarz method is used as the preconditioner for the global GMRES solver in each propagation step.

In the rest of the paper, we introduce a "reuse" strategy for solving the sequence of linear systems based on a domain decomposition method in which many subdomain proconditioners can be reused and a Krylov subspace method whose initial vector is constructed by a "crack-extension" of the solution of the previous linear system.

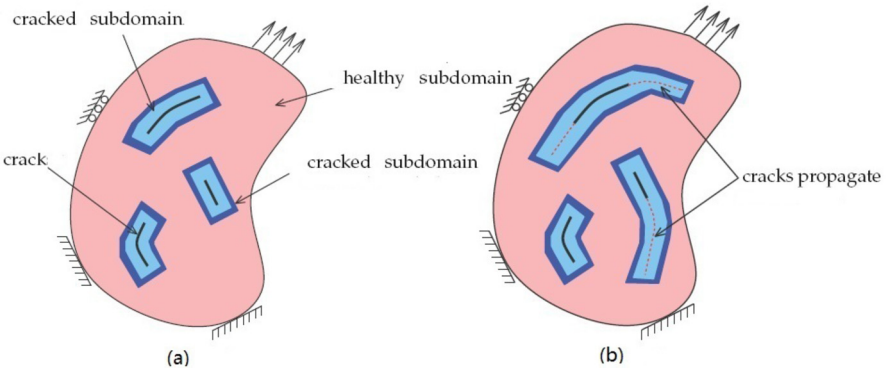

Fig. 5. Illustration of the domain decomposition approach. A healthy subdomain only contains the standard nodes, while cracked subdomains contain the enriched nodes. (a) Initial phase - each crack is contained in a subdomain. (b) Final phase - cracks propagate and the subdomains that contain the cracks are adaptively updated.

4. Recycling domain decomposition preconditioners and a Krylov subspace method with estimated initial guess

To apply DDM for the linear systems arising from crack propagation problems discretized by geometrical XFEM, it is important to choose a suitable strategy to decompose the degrees of freedom into subsets. In [4], the domain is partitioned into cracked subdomains and a healthy subdomain for the topological XFEM. In this partition, the whole crack line is involved in a cracked subdomain, see Fig. 5(a). In [29], two adaptive subdomain updating techniques (the level set based technique and the neighbors-based technique) are used to generate new cracked subdomains at each time step. In this domain decomposition approach, not only extra search algorithms are needed, but also the sizes of cracked subdomains become larger and larger, that increases the computational cost considerably, see Fig. 5(b).

In this paper, we apply a decomposition strategy for crack propagations, which separates the DOFs of the branch functions and the remaining DOFs, including the DOFs of standard basis functions, the Heaviside function and the Junction function.

4.1. A crack-tip decomposition

As discovered in [30], the tip enhancement has a huge impact on the eigenvalue distribution of the stiffness matrix near zero, and the small eigenvalues of the stiffness matrix are all associated with the crack tips. In our DOF decomposition, we separate all DOFs associated with the crack tips from other DOFs, but the DOFs associated with the crack lines are treated the same as the other nodes in the finite element mesh. It means that we need some crack tip subdomains covering the tip regions; only the tip, not the whole crack line.

The domain decomposition strategy is described as follows; see also Fig. 6.

- The crack tip subdomains. Suppose there are M crack tips. For the j^{th} tip, we introduce a subdomain Ω_j consisting of all the DOFs of the branch enrichment functions, i.e., the blue boxes in Fig. 6.
- To obtain the regular subdomains, we partition the global domain in a checker-board fashion into subdomains $\Omega_1, \ldots, \Omega_N$, and each subdomain consists of the standard DOFs, the DOFs of the Heaviside and the Junction enrichment functions together, but not the DOFs of the branch enrichment functions, i.e., the black subdomains in Fig. 6.
- In order to apply the overlapping domain decomposition method, all the subdomains are extended outward to include δ layers of nodes from neighboring subdomains to obtain the overlapping subdomains $\Omega_i^\delta (i = 1, \ldots, N)$ and $\Omega_j^\delta (j = 1, \ldots, M)$. Here δ is an integer ≥ 0. The overlapping crack tip subdomains Ω_j^δ include not only all the DOFs in Ω_j, but also the standard DOFs and some Heaviside enriched DOFs in the δ layer. In other words, the computational mesh Ω_h, together with all DOFs defined on it, is decomposed into overlapping subdomains

$$\Omega_h = \sum_{i=1}^{N} \Omega_i^\delta \cup \sum_{j=1}^{M} \Omega_j^\delta.$$

It should be pointed out that when cracks propagate, we still keep the original regular subdomains unchanged, even though more element nodes are enriched with the Heaviside and possibly the Junction functions. We only need to modify the crack tip subdomains around the new crack tips, no extra search is needed. Moreover, the sizes of crack tip subproblems do not increase as the cracks propagate, which saves greatly the computational cost.

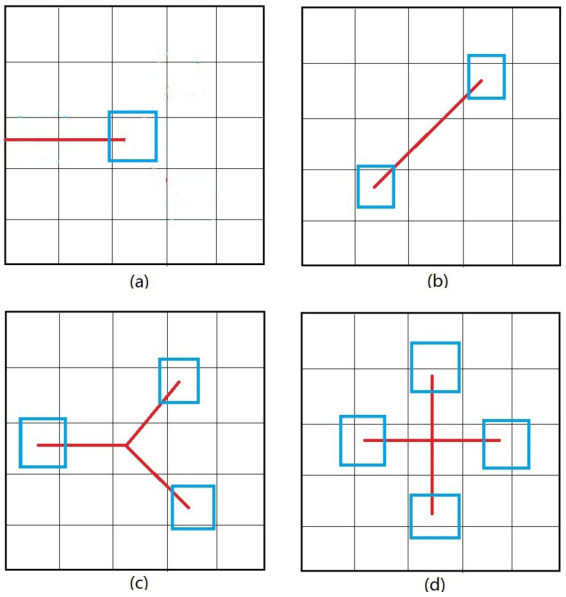

Fig. 6. The domain decomposition strategy. The red lines denote the cracks. The DOFs are decomposed into some regular subdomains (black subdomains) and crack tip subdomains (blue subdomains). There is no special treatment for the crack lines (not including the tips). (a) Uniaxial tensile boundary crack, (b) Central inclined crack, (c) T-type crack, and (d) Crosscut crack.

The authors of [29] constructed a Schwarz-AMG preconditioner for crack propagations modeled by the topological XFEM, in which kinks that occur within an element due to the propagation are smoothed out and the element is considered as fully fractured (straight crack). Here, we adopt the geometrical XFEM to discretize problems with or without kinks.

4.2. Additive and restricted additive Schwarz preconditioners

Based on the above-mentioned decomposition of the mesh, we present a additive Schwarz (AS) and a restricted additive Schwarz (RAS) preconditioner for the Krylov subspace method GMRES [17] for solving the sequence of linear systems (11).

Algorithm 1 Additive Schwarz preconditioned Krylov subspace method.

Solve a sequence of systems of varying sizes

$$A^k (M_{AS}^k)^{-1} \tilde{u}^k = b^k, \quad u^k = (M_{AS}^k)^{-1} \tilde{u}^k, \quad k = 0, 1, \cdots$$

by a Krylov subspace method with an initial guess u_0^k obtained by a modified u^{k-1} (except $u_0^0 = 0$), where the preconditioner at the k^{th} propagation step is defined by

$$(M_{AS}^k)^{-1} = \sum_{i=1}^{N} R_i^\delta (A_i^k)^{-1} R_i^\delta + \sum_{j=1}^{M} R_j^\delta (A_j^k)^{-1} R_j^\delta,$$

where $(A_i^k)^{-1} (i = 1, \cdots, N)$ is a subspace inverse of A_i^k and is solved inexactly as usual (such as ILU or multigrid), but the subdomain systems corresponding to $A_j^k (j = 1, \cdots, M)$ are solved exactly.

Let $\delta \geq 0$ be an integer denoting the level of overlap, $\delta = 0$ means that there is no overlap between the neighboring subdomains. We first define the subdomain restriction matrix R_i^δ which is a sub-identity matrix whose diagonal entries are one or zero, and $R^\delta u^k$ keeps the components of u^k in Ω_i^δ unchanged, and zeros out all other components. The regular subdomain stiffness matrix A_i^k ($A_i^k = A^k|_{\Omega_i^\delta}$, $i = 1, \cdots, N$) and the crack tip subdomain stiffness matrix A_j^k ($A_j^k = A^k|_{\Omega_i^\delta}$, $j = 1, \cdots, M$) at the k^{th} propagation step are defined as follows:

$$A_i^k = R_i^\delta A^k R_i^\delta, \quad A_j^k = R_j^\delta A^k R_j^\delta.$$

The AS and RAS preconditioners are described in Algorithm 1 and Algorithm 2, respectively; see [6,7] for details.

Algorithm 2 Restricted additive Schwarz preconditioned Krylov subspace method.

Solve a sequence of systems of varying sizes

$$A^k(M^k_{RAS})^{-1}\tilde{u}^k = b^k, \quad u^k = (M^k_{RAS})^{-1}\tilde{u}^k, \quad k = 0, 1, \cdots$$

by a Krylov subspace method with an initial guess u^k_0 obtained by a modified u^{k-1} (except $u^0_0 = 0$), where the preconditioner at the k^{th} propagation step is defined by

$$(M^k_{RAS})^{-1} = \sum_{i=1}^{N} R^0_i (A^k_i)^{-1} R^\delta_i + \sum_{j=1}^{M} R^0_j (A^k_j)^{-1} R^\delta_j,$$

where $(A^k_i)^{-1}(i = 1, \cdots, N)$ is a subspace inverse of A^k_i and is solved inexactly as usual (such as ILU or multigrid), but the subdomain systems corresponding to $A^k_j(j = 1, \cdots, M)$ are solved exactly.

Remark 1. Note that there are several ways to apply a preconditioner to a linear system including left, right, and also double-sided preconditioning when two preconditioners can be applied to a system. In this paper, we only consider the right-preconditioned GMRES because the right-preconditioned residual is the same as the residual of the original problem without preconditioning. See chapter 9 of [17] for details.

We should point out that when cracks propagate, some of the subdomain matrices do not change, which can be reused in the next propagation steps.

Remark 2. One may argue that the use of a direct solver on the crack tip subdomain may be computationally too expensive, we point out that the crack tip subdomain is relatively small compared with the overall problem, and therefore, this step is fairly inexpensive. Our experiments indicate, unfortunately, inexact solvers such as ILU are not appropriate for the crack tip problem as they will increase the number of iterations drastically. Furthermore, only a very small number of elements surrounding the crack tips are enriched by the branch functions, the scales of the crack tip subproblems are still small in 3D simulations, and our method would also be applicable.

4.3. GMRES with estimated initial guesses

As mentioned earlier, the linear systems in the sequence (11) are of difference sizes that makes it is impossible to use the recycling GMRES, however, the systems have certain inner connections in the sense that the solutions of two consecutive systems are not too far from each other.

Consider two algebraic systems at the k^{th} and $(k+1)^{th}$ propagation steps,

$$A^k u^k = b^k, \qquad A^{k+1} u^{k+1} = b^{k+1},$$

and the second one is the further crack of the first one. u^{k+1} is larger than u^k in terms of the dimensions. u^{k+1} can be written as $u^{k+1} = (z^{k+1}_1, z^{k+1}_2)$, here z^{k+1}_1 is associated with old cracks and has the same dimension as u^k. It is reasonable to guess that most components of z^{k+1}_1 are close to the corresponding components of u^k. Below we present some simple ways to extract some useful information from the solution of the first system to be used as the initial guess when solving the second system.

In XFEM, the DOF of the numerical solution u^k includes two parts, the standard FEM solution u^k_{FEM} and the enhanced solution u^k_{Enr}

$$u^k = [u^k_{FEM} \qquad u^k_{Enr}]$$

The usual initial guess u^{k+1}_0 at the $(k+1)^{th}$ propagation step may be chosen as

$$u^{k+1}_0 = [0 \qquad 0 \qquad 0], \tag{12}$$

where the first two zero vectors correspond to the DOF of u^k_{FEM} and u^k_{Enr}, and the third zero vector corresponds to the new DOFs from the growth of the cracks. However, based on the observation that the solution of the system is related to the solution of the previous system, we may want to consider the second choice of the initial guess as

$$u^{k+1}_0 = [u^k_{FEM} \qquad u^k_{Enr} \qquad 0]. \tag{13}$$

In addition to (12) and (13), we propose a more sophisticated initial guess. For this purpose, we introduce an auxiliary crack tip subproblem at the k^{th} propagation step to construct u^{k+1}_0, which can be described as follows. For each crack tip k_{tip}, the auxiliary subdomain $\Omega^i_{k,Auxil}$ includes part of the Heaviside enriched nodes at the k^{th} and $(k+1)^{th}$ propagation step, and all the branch enriched nodes around the crack tips k_{tip} and $(k+1)_{tip}$, see the blue boxes in Fig. 7.

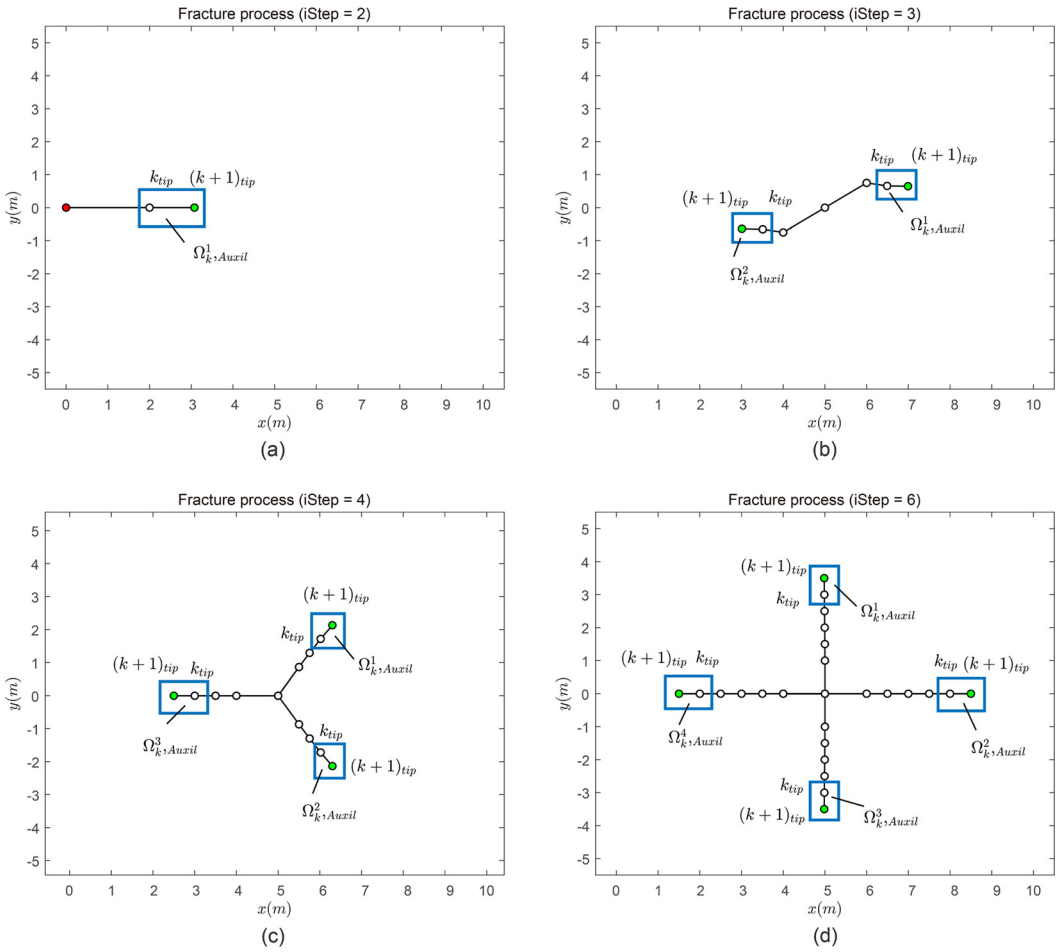

Fig. 7. The auxiliary crack tip subdomains $\Omega^i_{k,Auxil}(i = 1, \cdots, 4)$. The green circles denote the crack tips at the $(k+1)^{th}$ propagation step. (a) an uniaxial tensile boundary crack propagation, (b) a central inclined crack propagation, (c) a T-type crack propagation and (d) a crosscut crack propagation.

The auxiliary subdomain stiffness matrix $A^i_{k,Auxil}$ is defined as

$$A^i_{k,Auxil} = A^k|_{\bar{\Omega}^i_{k,Auxil}},$$

where $\bar{\Omega}^i_{k,Auxil} = \Omega^i_{k,Auxil} \cup \partial\bar{\Omega}^i_{k,Auxil}$ and A^k is the global stiffness matrix at the k^{th} propagation step. Although $\Omega^i_{k,Auxil}$ involves the next crack tip $(k+1)_{tip}$, the enriched DOFs of the $(k+1)^{th}$ propagation step are not included in $A^i_{k,Auxil}$.

Set

$$b^i_{k,Auxil} = b^k|_{\bar{\Omega}^i_{k,Auxil}},$$

where b_k is the right-hand side at the k^{th} propagation step. We solve the following auxiliary crack tip subproblem

$$A^i_{k,Auxil} u^i_{k,Auxil} = b^i_{k,Auxil}.$$

Note that, the above auxiliary crack tip subproblem is relatively small compared with the overall problem, and a direct solver is used here, which is fairly inexpensive. Then, we extract the Heaviside DOFs from $u^i_{k,Auxil}$, and denote it as $u_{k,Auxil,Heav}$. Then, we introduce the third choice of the initial guess u^{k+1}_0 as

$$u^{k+1}_0 = [u^k_{FEM} \quad 0 \quad u_{k,Auxil,Heav} \quad 0]. \tag{14}$$

The efficiency of different initial guesses u^{k+1}_0 will be studied in the following section on numerical experiments. The flow chart of the entire process for the proposed crack propagation simulation shown in Fig. 8.

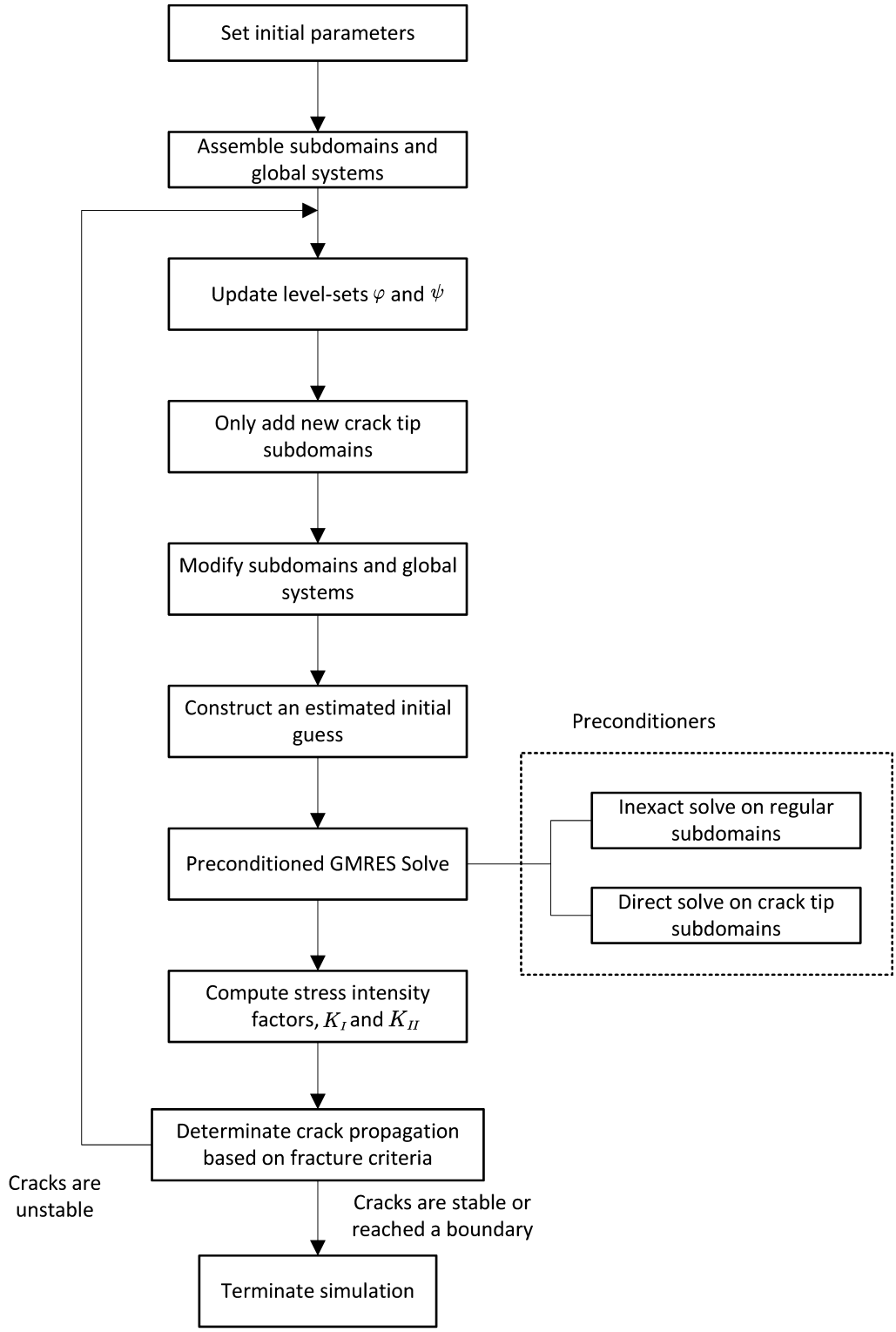

Fig. 8. Flow chart of the process for the proposed crack propagations.

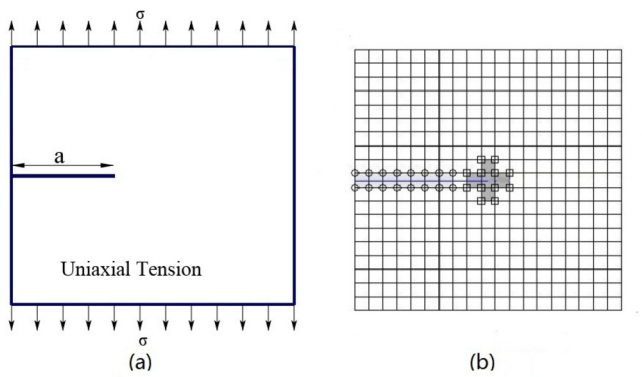

Fig. 9. The initial geometry (a) and the mesh (b) for the uniaxial tensile boundary crack problem. In (b), the squares □ represent tip enriched nodes and the circles ○ represent heaviside enriched nodes.

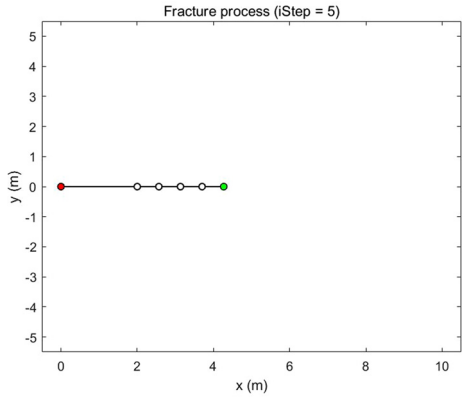

Fig. 10. The uniaxial tensile boundary crack propagation. The black line denotes the crack. The red circle ○ represents the starting point of the crack, the white circles ○ represent the propagation points and the green circle ○ represents the propagation point at istep=5.

Remark 3. The idea of using some previous information to accelerate the present iterations can also be found in other fields. For example, in fluid dynamics, people have used information of previous time steps which follow a similar idea of recycling information of a nearby system, e.g., by projection as proposed in P.F. Fischer [9], or by extrapolation from old values as proposed in section 5.1 of B. Krank et al. [11].

5. Numerical experiments

In this section, we present some numerical experiments to illustrate the performance of the proposed strategy. In the XFEM implementation, the level set approach is used in the crack intersection problems (see Section 2.2). To simplify the study, we propagate cracks by an increment of Δa, which is defined as the largest element diameter in the mesh. We consider four examples: (i) an uniaxial tensile boundary crack growth problem, (ii) a central inclined crack propagation problem, (iii) a T-type crack propagation problem, and (iv) a crosscut crack propagation problem. In all the experiments, the preconditioner is used as a right preconditioner, GMRES is re-started at 30, and the relative stopping tolerance is chosen as 10^{-7}. For all the test problems, we assume the material is under the plane stress condition. All the numerical experiments are implemented in MATLAB.

5.1. Uniaxial tensile boundary crack propagation

We consider the classic problem of an uniaxial tensile boundary crack, in which the crack propagates from a point on the boundary following a mode I opening. The side length of the square plate is $10m$. Its Young's modulus is $E = 60.89GPa$, and the Poisson's ratio is $\nu = 0.3$. The plate is subject to a pure tension applied on the top and bottom of the plate, $\sigma = 1MPa$. The right boundary is fixed, and the left boundary is free. The length of an initial crack is $2m$, see Fig. 9.

We first present a calculation obtained on a 70×70 mesh. The propagation of the uniaxial tensile boundary crack is shown in Fig. 10. Plots of the subdomains following the crack during the propagation as well as plots of the von Mises

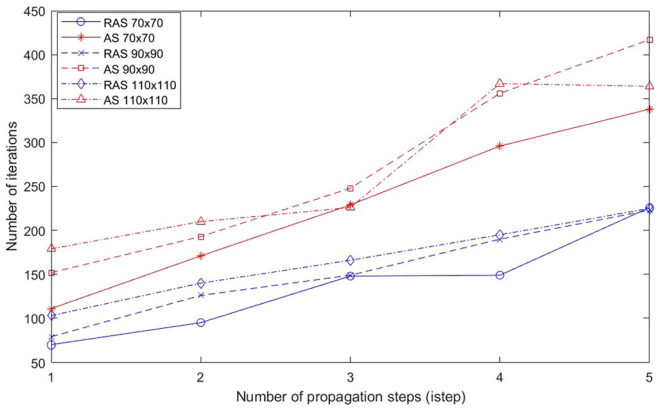

Fig. 11. Convergence of AS and RAS preconditioners for various meshes for an uniaxial tensile boundary crack problem as a function of the propagation step. The domain is decomposed into 4×4 regular subdomains plus one crack tip subdomain.

stresses at three different propagation steps are provided as snapshots in Fig. 12, in which we can see that all the regular subdomains remain unchanged, and only a crack tip subdomain is added around the new crack tip as crack propagations. No extra search algorithm is needed to update the subdomains.

Next, we test the convergence of different preconditioners. In the AS and RAS preconditioners, the exact solver is used in the crack tip subdomain and an inexact solver (ILU(0) with a drop tolerance 10^{-3}) is used in regular subdomains. For the iterative solver, Fig. 11 shows the number of iterations required by the different preconditioners for the convergence against the propagation step of the crack with the initial guess (12). We can see that the number of iterations of the RAS preconditioner is fewer than that of the AS preconditioner. Some comparison results of the convergence rates of AS and RAS can be found in [10]. Also, as expected, the slope of the curve increases when the mesh is refined.

Finally, we study the impact of different initial guesses (12)-(14). From Table 1, we see that the use of the new initial guess (14) can reduce the number of iterations remarkably. On the 110×110 mesh partitioned into 65 subdomains, the saving with the initial guess (14) is about 70% compared with (12). When we increase the overlap, the number of iterations is reduced with all three initial guesses as expected. Moreover, when we increase the number of subdomains, the number of iterations with the initial guesses (12) and (13) increase significantly, but the number of iterations with the initial guess (14) increase only slightly.

Remark 4. It should be pointed out that even for the simple uniaxial tensile boundary crack growth problem, when we use GMRES method with non-preconditioner or with the traditional ILU preconditioner, the convergence is very slow, and thousands of iterations are often needed. Therefore, we don't list the relevant results here.

5.2. Central inclined crack propagation

The second experiment is a central inclined crack propagation problem. The side length of the square plate is $10m$, its Young's modulus is $E = 20GPa$, and the Poisson's ratio is $\nu = 0.3$. The boundary of the region is subject to two tensile loads $\sigma_1 = 1MPa$, $\sigma_2 = 2MPa$. The length of the initial crack is $1.25m$, $\beta = \frac{\pi}{6}$; see Fig. 13.

The computed propagation of the central inclined crack is shown in Fig. 14. Plots of the subdomains following the crack during the propagation, as well as plots of the von Mises stresses at three different propagation steps, are provided as snapshots in Fig. 16, in which we can see that all the regular subdomains remain the same, and only two crack tip subdomains are added around new crack tips as the crack grows. There is no need to use any extra search algorithm to update the subdomains.

In the AS and RAS preconditioners, the same as in the previous test, exact solvers are used in the crack tip subdomains and an inexact solver (ILU(0) with a drop tolerance 10^{-5}) is used in regular subdomains. Compared with the horizontal crack, there are more element nodes along the inclined crack that are enriched with the Heaviside enrichment function. So, we need to solve the regular subproblems more accurately for better performance. Fig. 15 shows the number of iterations required by the different solvers for each propagation step. We see clearly that the number of iterations of RAS on the finest mesh 110×110 is fewer than that of AS on the coarsest mesh 70×70. The results strong indicate that the RAS preconditioner is much more effective than the AS preconditioner in this case.

From Table 2, we see that the use of the new initial guess (14) can reduce the number of iterations remarkably. On the finest mesh 110×110, when the number of subdomains is 66, the saving with the initial guess (14) is around 77% compared with (12). The number of iterations is reduced with all three initial guesses as the overlap is increased. Moreover, when we increase the number of subdomains, the number of iterations with the initial guess (14) tends to be stable.

Table 1
The number of iterations for the uniaxial tensile boundary crack propagation when using the RAS preconditioner. The domain is decomposed into $m \times m$ regular subdomains plus one crack tip subdomain, and different initial guesses (12)-(14) are used respectively. The number of iterations are presented in black when the mesh is 70×70, blue when the mesh is 90×90, and red when the mesh is 110×110. (For interpretation of the colors in the table(s), the reader is referred to the web version of this article.)

subdomains $4 \times 4 + 1 = 17$, $overlap = 2$.									
istep	initial guess (12)			initial guess (13)			initial guess (14)		
1	70	79	103	-	-	-	-	-	-
2	76	86	108	58	67	69	42	46	51
3	87	106	116	63	70	77	44	47	44
4	97	115	137	70	76	79	43	42	42
6	114	134	144	88	85	82	50	50	51
8	136	143	161	110	105	104	61	61	63
subdomains $4 \times 4 + 1 = 17$, $overlap = 4$.									
istep	initial guess (12)			initial guess (13)			initial guess (14)		
1	57	68	71	-	-	-	-	-	-
2	61	72	77	47	53	60	39	41	44
3	67	74	79	54	57	54	40	41	42
4	71	79	88	55	59	59	37	41	42
6	81	77	93	60	67	71	43	38	40
8	101	102	113	75	69	81	53	51	50
subdomains $6 \times 6 + 1 = 37$, $overlap = 2$.									
istep	initial guess (12)			initial guess (13)			initial guess (14)		
1	106	130	135	-	-	-	-	-	-
2	106	134	145	69	90	105	46	43	67
3	128	149	149	71	97	105	48	47	45
4	136	149	165	80	103	109	45	45	40
6	140	175	186	105	110	115	55	51	54
8	158	200	206	134	129	132	68	64	69
subdomains $8 \times 8 + 1 = 65$, $overlap = 2$.									
istep	initial guess (12)			initial guess (13)			initial guess (14)		
1	117	142	180	-	-	-	-	-	-
2	137	145	157	73	100	105	47	43	75
3	139	155	186	101	109	101	50	45	41
4	153	159	210	106	111	112	50	50	50
6	177	191	223	120	126	133	56	56	58
8	224	239	245	149	140	140	70	70	70

5.3. T-type crack propagation

The third experiment is a T-type crack propagation problem. The side length of the square plate is $10m$, its Young's modulus is $E = 40GPa$, and the Poisson's ratio is $\nu = 0.3$. The top and bottom boundaries of the region are subject to the tensile loads $\sigma = 1MPa$, $a = 1m$, $b = 1m$, $\theta = \frac{\pi}{4}$; see Fig. 17.

The computed propagation of the T-type crack is shown in Fig. 18. Plots of the subdomains following the crack during the propagation as well as plots of the von Mises stresses at three different propagation steps are provided as snapshots in Fig. 20, in which we can see that all the regular subdomains remain the same, and only three crack tip subdomains are added around new crack tips as the crack grows.

The same as in the previous tests, an inexact solver (ILU(0) with a drop tolerance 10^{-7}) is used in regular subdomains. Fig. 19 shows the number of iterations by different solvers for each propagation step. We can see that, in the finest mesh, the slope of the curve is very steep in the AS preconditioner, and that of the RAS preconditioner is relatively gentle as the crack propagates.

Table 3 shows that the new initial guess (14) can reduce the number of iterations remarkably. On the 110×110 mesh with 67 subdomains, the saving is around 77%. When we increase the number of subdomains, although the number of iterations when using the new initial guess (14) changes slightly, the number of iterations decreases significantly comparing with the other initial guesses.

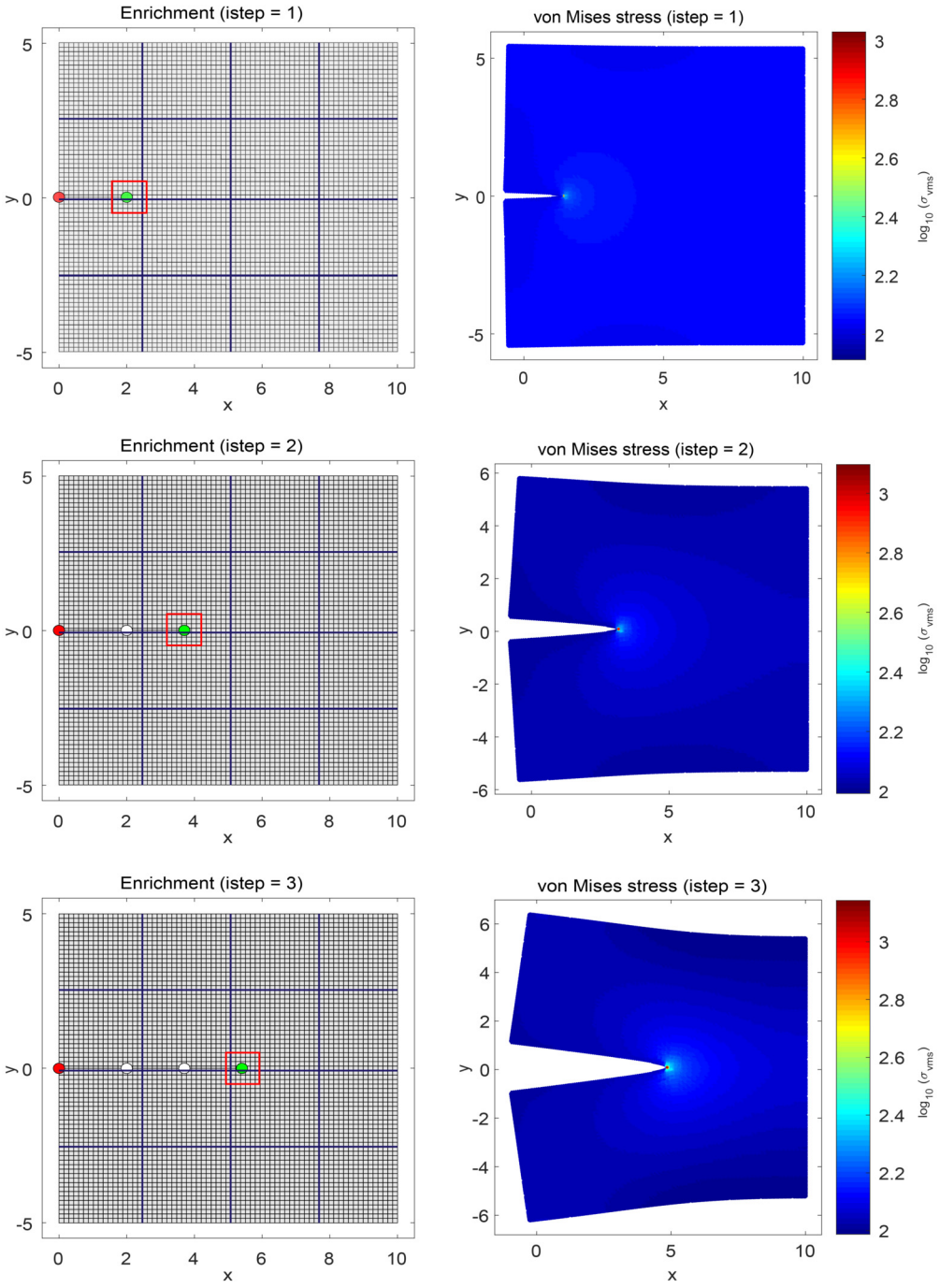

Fig. 12. The uniaxial tensile boundary crack propagation problem. Snapshots of subdomains (left) and von Mises stresses (right) computed at different propagation steps (istep=1, 2 and 3). The black line denotes the crack. The domain is decomposed into 4×4 regular subdomains (blue subdomains) plus one crack tip subdomain (the red subdomain). The mesh is 70×70.

5.4. Crosscut crack propagation

The last experiment is the crosscut crack propagation problem. The side length of the square plate is $10m$, its Young's modulus is $E = 20GPa$, and the Poisson's ratio is $\nu = 0.3$. The boundary of the region is subject to the tensile loads $\sigma = 1MPa$. The size of the crack is $a = 1m$, see Fig. 21.

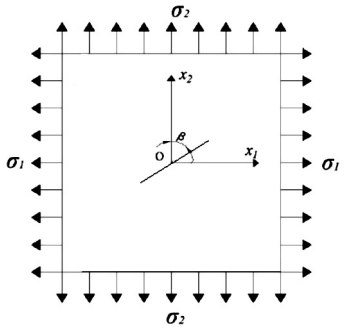

Fig. 13. The initial geometry of the central inclined crack propagation problem.

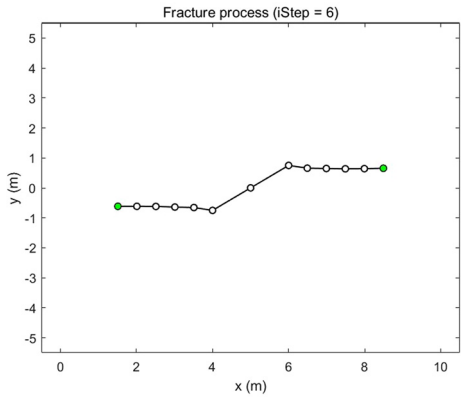

Fig. 14. The central inclined crack propagation. The black line denotes the crack. The white circles ○ represent the propagation points and the green circles ○ represent the propagation point at istep=6.

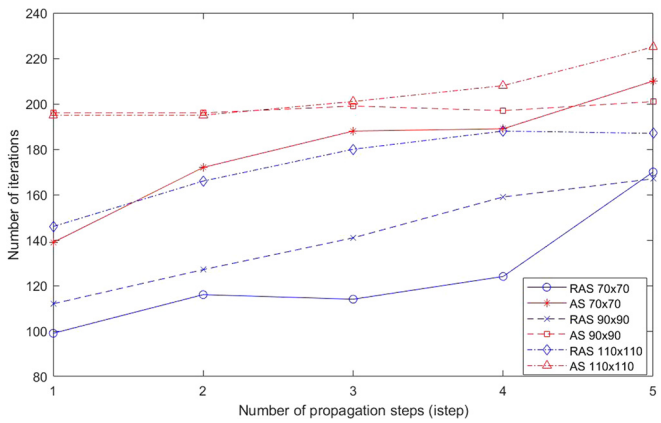

Fig. 15. Convergence of AS and RAS preconditioners for meshes of different sizes for the central inclined crack propagation problem as a function of the propagation step. The domain is decomposed into 4×4 regular subdomains plus two crack tip subdomains.

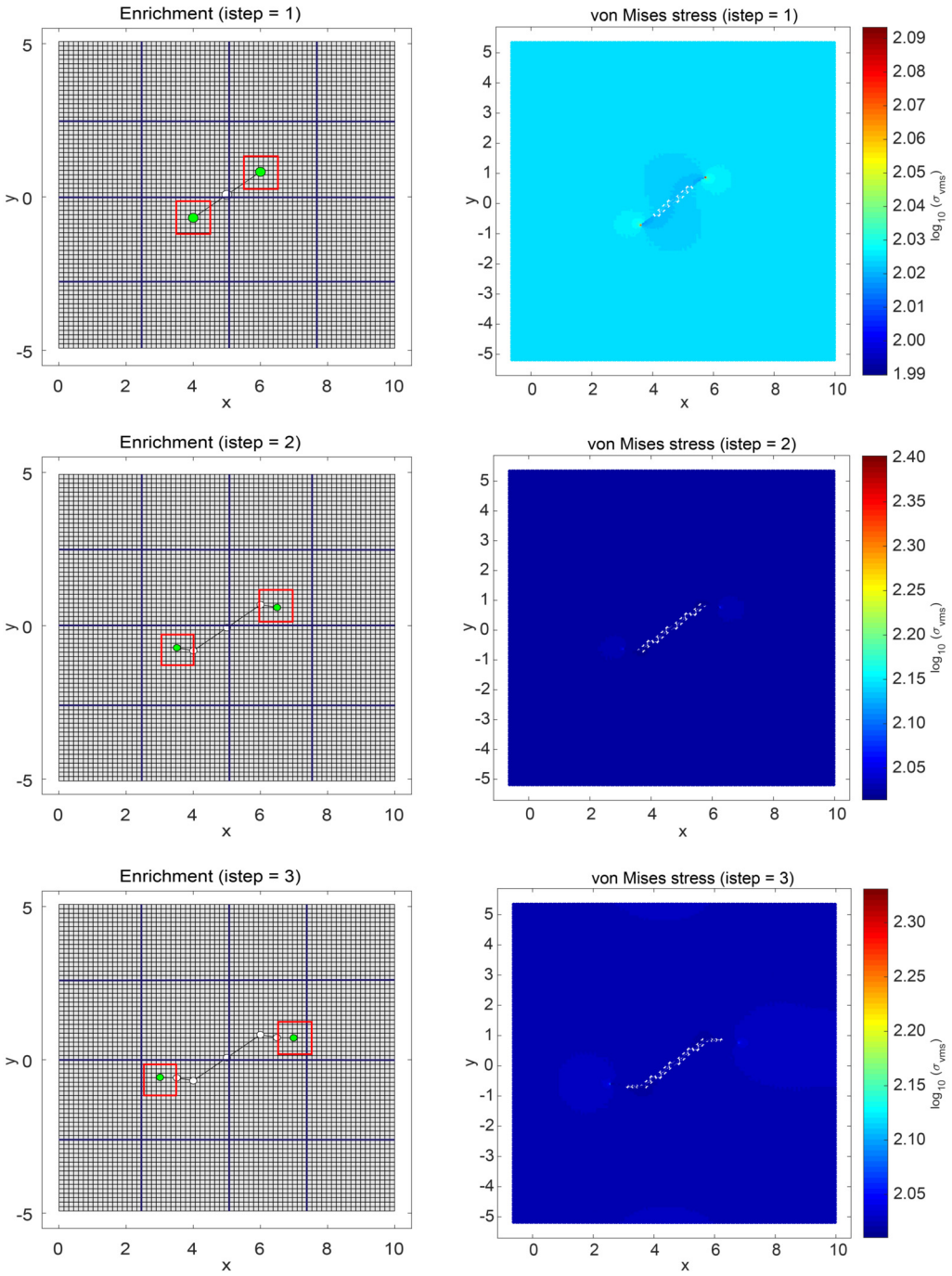

Fig. 16. The central inclined crack propagation problem. Snapshots of subdomains (left) and von Mises stresses (right) computed at different propagation steps (istep=1, 2 and 3). The black line denotes the crack. The domain is decomposed into 4×4 regular subdomains (blue subdomains) plus two crack tip subdomains (the red subdomains). The mesh is 70×70.

Table 2
The number of iterations for the central inclined crack propagation with the RAS preconditioner. The domain is decomposed into $m \times m$ regular subdomains plus two crack tip subdomains, and different initial guesses (12)-(13) are used respectively. The number of iterations are presented in black when the mesh is 70×70, blue when the mesh is 90×90, and red when the mesh is 110×110.

subdomains $4 \times 4 + 2 = 18$, $overlap = 2$.									
istep	initial guess (12)			initial guess (13)			initial guess (14)		
1	73	95	110	-	-	-	-	-	-
2	80	111	129	63	80	100	37	47	57
3	80	128	157	59	76	98	43	49	57
4	92	137	173	62	79	115	50	59	58
5	112	159	178	65	102	115	50	67	60
6	178	165	192	85	102	128	59	59	58

subdomains $4 \times 4 + 2 = 18$, $overlap = 4$.									
istep	initial guess (12)			initial guess (13)			initial guess (14)		
1	58	65	76	-	-	-	-	-	-
2	63	83	99	53	58	69	31	43	50
3	63	80	114	52	57	63	34	41	51
4	70	78	119	55	59	74	43	49	51
5	69	102	119	56	68	77	44	53	51
6	98	103	132	80	75	79	46	50	52

subdomains $6 \times 6 + 2 = 38$, $overlap = 2$.									
istep	initial guess (12)			initial guess (13)			initial guess (14)		
1	99	135	163	-	-	-	-	-	-
2	103	171	162	85	108	119	37	45	74
3	125	161	207	81	116	135	48	57	77
4	145	165	214	84	125	137	56	73	63
5	142	200	208	89	121	137	55	75	62
6	252	223	227	171	141	156	57	66	70

subdomains $8 \times 8 + 2 = 66$, $overlap = 2$.									
istep	initial guess (12)			initial guess (13)			initial guess (14)		
1	135	148	174	-	-	-	-	-	-
2	156	169	236	105	120	133	39	49	78
3	157	167	270	102	125	146	55	52	76
4	167	207	285	110	134	170	59	82	67
5	172	248	296	114	143	170	61	82	63
6	326	262	300	188	150	203	60	70	67

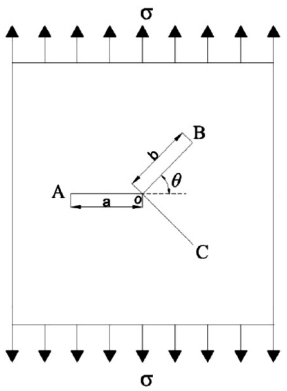

Fig. 17. The initial geometry of the T-type crack propagation problem.

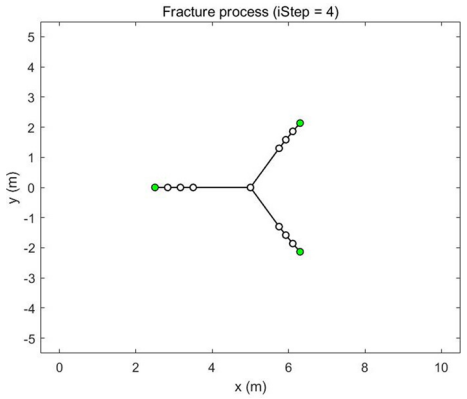

Fig. 18. The T-type crack propagation. The black line denotes the crack. The white circles ○ represent the propagation points and the green circles ○ represent the propagation point at istep=4.

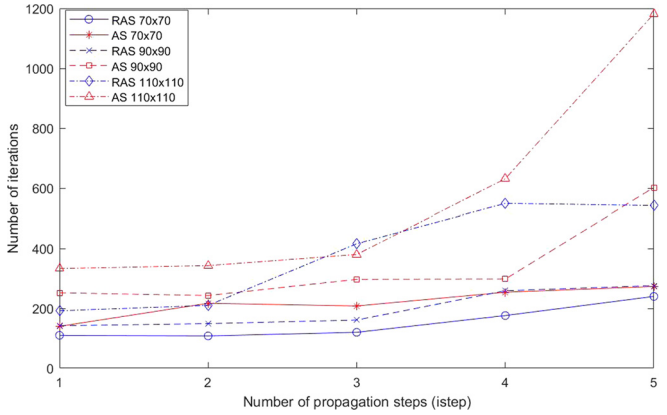

Fig. 19. Convergence of AS and RAS preconditioners on meshes of different sizes for a T-type crack problem as a function of the propagation step. The domain is decomposed into 4×4 regular subdomains plus three crack tip subdomains.

The computed propagation of the crosscut crack is shown in Fig. 22. Plots of the subdomains following the crack during the propagation as well as plots of the von Mises stresses at three different propagation steps are provided as snapshots in Fig. 24, in which we can see that all the regular subdomains remain the same, and only four crack tip subdomains are added around new crack tips as the crack grows.

In the test, an inexact solver (ILU(0) with a drop tolerance 10^{-3}) is used in regular subdomains. Fig. 23 shows the number of iterations by different solvers for each propagation step. The RAS preconditioner is more effective than the AS preconditioner as before.

From Table 4, we show that the initial guess (14) can reduce the number of iterations by as much as 84% for a 110×110 mesh partitioned into 68 subdomains. When we refine the mesh or increase the number of subdomains, the number of iterations of the initial guess (14) is stable in this model.

Remark 5. In all simulations, an inexact solver ILU(0) with different drop tolerance is used in regular subdomains. In the first and forth crack propagation problems, the cracks are parallel to the coordinate axis, only the mesh nodes on the adjacent lines below or above the cracks are enriched by the Heaviside function. In the second and third crack propagation problems, the cracks are inclined, more mesh nodes around the cracks are enriched by the Heaviside function, that results in more ill-conditionness in the linear systems. Therefore, in order to achieve acceptable performance, we need to solve the subproblems in regular subdomains more accurately; i.e., using inexact ILU(0) with smaller drop tolerances.

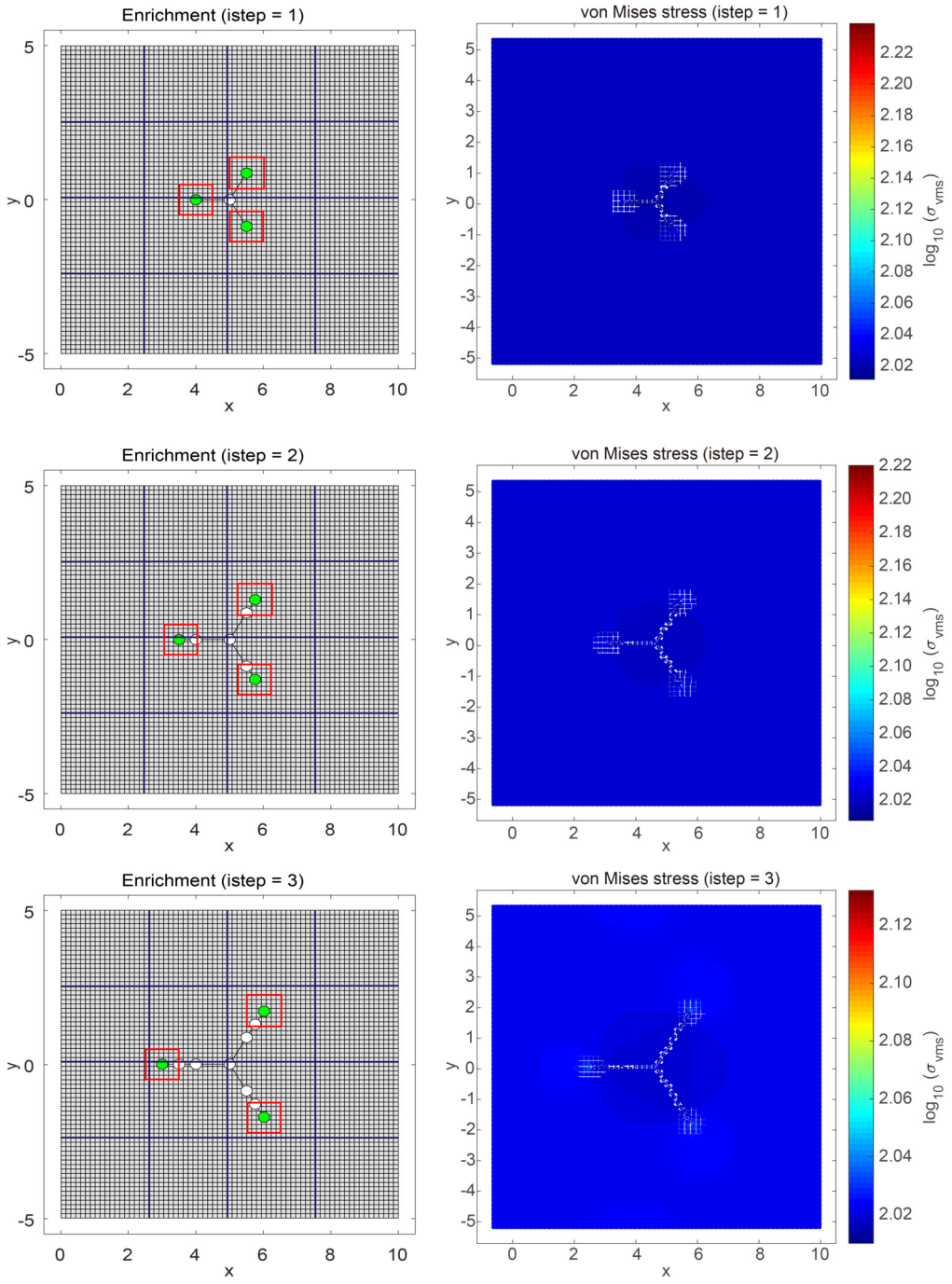

Fig. 20. The T-type crack propagation problem. Snapshots of subdomains (left) and von Mises stresses (right) computed at different propagation steps (istep=1, 2 and 3). The domain is decomposed into 4×4 regular subdomains (blue subdomains) plus three crack tip subdomains (the red subdomains). The mesh is 70×70.

Table 3
The number of iterations for the T-type crack propagation problem with the RAS preconditioner. The domain is decomposed into $m \times m$ regular subdomains plus three crack tip subdomains, and different initial guesses (12)-(14) are used respectively. The number of iterations are presented in black when the mesh is 70×70, blue when the mesh is 90×90, and red when the mesh is 110×110.

subdomains $4 \times 4 + 3 = 19$, $overlap = 2$.									
istep	initial guess (12)			initial guess (13)			initial guess (14)		
1	69	90	95	-	-	-	-	-	-
2	71	133	137	59	83	84	43	59	45
3	82	144	202	52	86	87	39	53	51
4	81	158	222	72	86	143	48	57	57
5	87	183	257	86	120	133	41	53	55
6	119	211	261	86	149	176	43	49	60

subdomains $4 \times 4 + 3 = 19$, $overlap = 4$.									
istep	initial guess (12)			initial guess (13)			initial guess (14)		
1	52	58	68	-	-	-	-	-	-
2	55	85	102	46	70	73	38	49	45
3	59	82	131	44	78	76	36	46	59
4	69	86	138	54	78	88	44	50	49
5	65	115	156	57	103	109	39	46	52
6	76	120	178	58	107	126	38	46	66

subdomains $6 \times 6 + 3 = 39$, $overlap = 2$.									
istep	initial guess (12)			initial guess (13)			initial guess (14)		
1	94	105	134	-	-	-	-	-	-
2	105	178	178	71	116	83	46	72	49
3	100	208	236	77	123	117	41	53	81
4	111	234	258	84	111	168	49	60	57
5	112	256	292	95	169	172	42	55	57
6	135	270	300	85	201	207	42	49	82

subdomains $8 \times 8 + 3 = 67$, $overlap = 2$.									
istep	initial guess (12)			initial guess (13)			initial guess (14)		
1	129	144	147	-	-	-	-	-	-
2	112	207	269	80	116	142	53	78	55
3	133	217	277	79	144	148	41	51	79
4	119	247	287	82	153	207	55	58	56
5	163	293	355	95	187	181	44	63	61
6	168	292	388	107	211	268	42	47	86

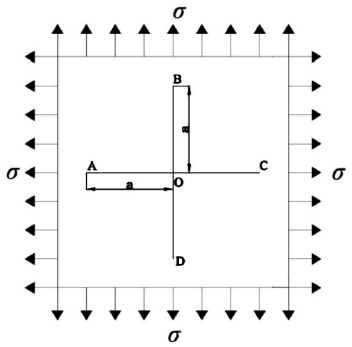

Fig. 21. The initial geometry of the crosscut crack propagation problem.

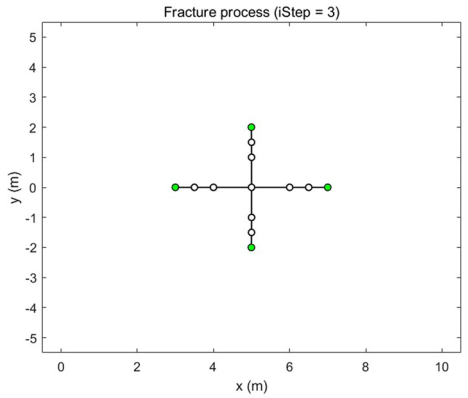

Fig. 22. The crosscut crack propagation. The black line denotes the crack. The white circles ○ represent the propagation points and the green circles ○ represent the propagation point at istep=3.

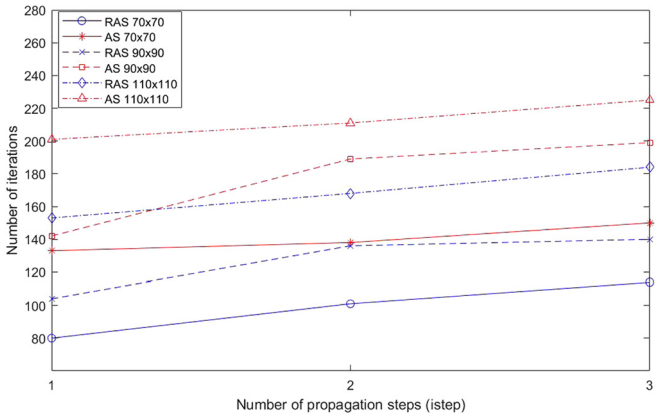

Fig. 23. Convergence of AS and RAS preconditioners for meshes of different sizes for a crosscut crack problem as a function of the propagation step. The domain is decomposed into 4×4 regular subdomains plus four crack tip subdomains.

6. Conclusions

In this paper, we introduced and studied some effective overlapping Schwarz preconditioners for the elastic crack propagation problems discretized by the geometric XFEM. A special decomposition of the domain is employed, in which the crack tip subdomains are separated from the crack line, and in the domain decomposition preconditioning, the crack tip subproblems are solved directly and the regular subproblems are solved inexactly. When cracks propagate, all the regular subdomains remain the same, and only new crack tip subdomains are added around new crack tips. This scheme avoids the repartitioning of the domain, and no extra search is needed to update the crack tip subdomains. To solve the sequence of large, sparse systems of linear equations of varying sizes, a Krylov subspace method is used with an initial guess built from the solution of the previous system with a local modification in the crack tip subspace. This initial guess constructed with an auxiliary tip subspace and the use of recycled preconditioner components can accelerate the convergence remarkably. The numerical experiments demonstrate the efficiency of our method. As the next step, we plan to extend the methods to three-dimensional problems.

CRediT authorship contribution statement

Xingding Chen: Conceptualization, software development and testing, manuscript preparation.
Xiao-Chuan Cai: Methodology, supervision, manuscript editing.

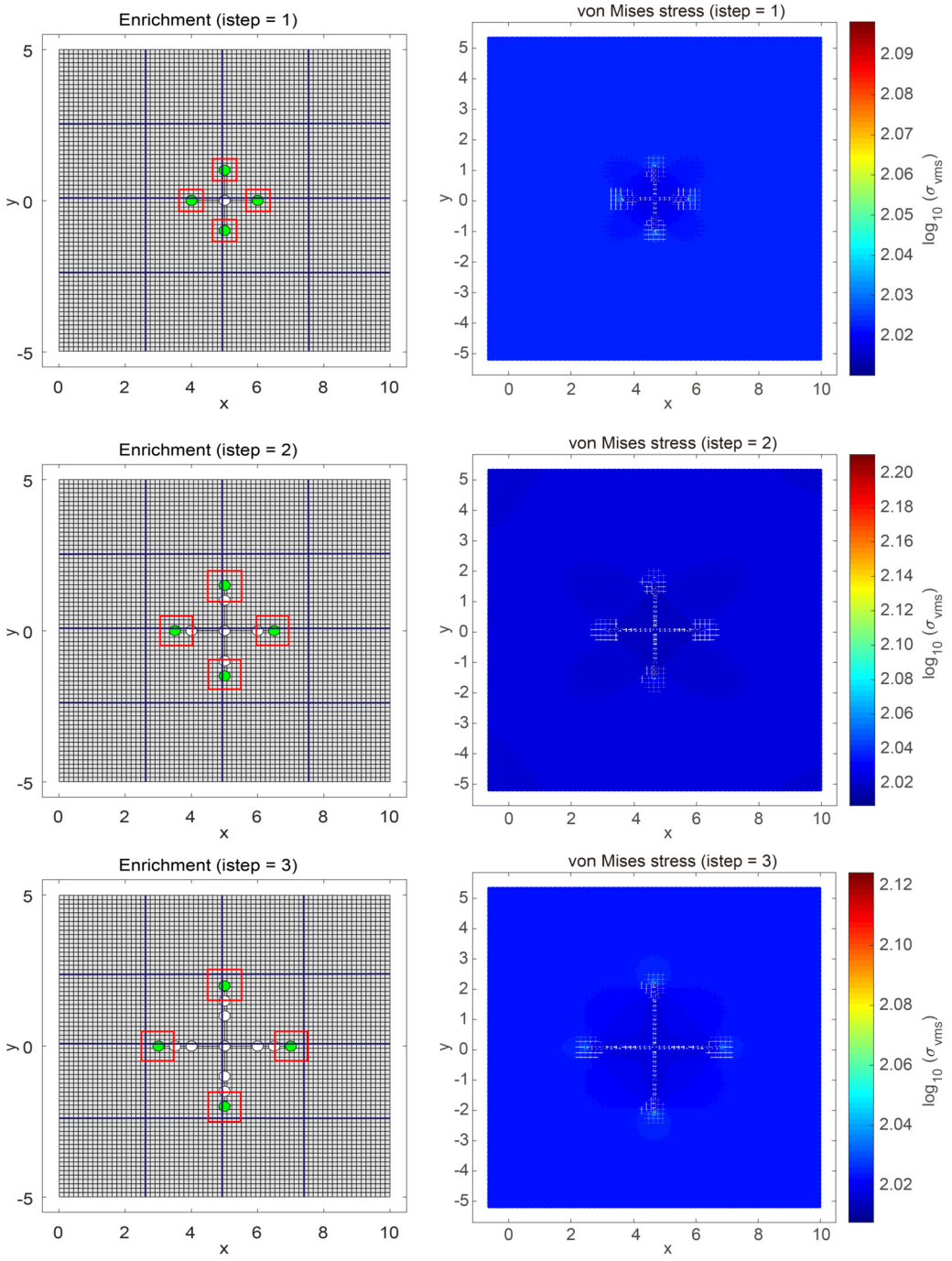

Fig. 24. The crosscut crack propagation problem. Snapshots of subdomains (left) and von Mises stresses (right) computed at different propagation steps (istep=1, 2 and 3). The domain is decomposed into 4×4 regular subdomains (blue subdomains) plus four crack tip subdomains (the red subdomains). The mesh is 110×110.

Table 4
The number of iterations of the crosscut crack propagation problem with the RAS preconditioner. The domain is decomposed into $m \times m + 4$ subdomains, which means $m \times m$ regular subdomains plus four crack tip subdomains, and different initial guesses (12)-(14) are used respectively. The number of iterations are presented in black when the mesh is 70×70, blue when the mesh is 90×90, and red when the mesh is 110×110.

subdomains $4 \times 4 + 4 = 20$, $overlap = 2$.									
istep	initial guess (12)			initial guess (13)			initial guess (14)		
1	80	104	153	-	-	-	-	-	-
2	101	136	148	74	85	93	51	49	55
3	114	140	184	73	83	115	45	55	57
4	114	162	197	77	87	140	50	54	47
5	122	168	213	81	114	150	52	57	47
6	128	207	304	95	153	193	55	52	56
subdomains $4 \times 4 + 4 = 20$, $overlap = 3$.									
istep	initial guess (12)			initial guess (13)			initial guess (14)		
1	78	102	109	-	-	-	-	-	-
2	82	110	135	60	82	85	39	42	52
3	79	131	157	71	81	89	44	52	45
4	98	127	166	75	81	115	49	51	51
5	100	148	192	73	84	144	49	54	45
6	120	172	232	81	114	179	51	53	55
subdomains $6 \times 6 + 4 = 40$, $overlap = 2$.									
istep	initial guess (12)			initial guess (13)			initial guess (14)		
1	111	148	183	-	-	-	-	-	-
2	106	140	167	76	83	113	56	54	53
3	118	171	212	80	94	137	48	57	57
4	139	180	208	86	110	148	55	47	46
5	149	184	232	88	129	164	53	59	44
6	179	231	338	111	186	173	58	51	55
subdomains $8 \times 8 + 4 = 68$, $overlap = 2$.									
istep	initial guess (12)			initial guess (13)			initial guess (14)		
1	139	180	193	-	-	-	-	-	-
2	135	183	204	77	111	124	60	55	47
3	139	194	216	84	121	143	48	60	53
4	168	200	199	90	139	158	57	48	47
5	176	179	238	110	158	159	56	60	42
6	185	329	348	126	205	189	63	52	55

Declaration of competing interest

The authors declare that they have no known competing financial interests or personal relationships that could have appeared to influence the work reported in this paper.

Acknowledgements

The authors would like to acknowledge the support from the National Natural Science Foundation of China grant G12071469.

References

[1] T. Belytschko, T. Black, Elastic crack growth in finite elements with minimal remeshing, Int. J. Numer. Methods Eng. 45 (1999) 601–620.
[2] T. Belytschko, R. Gracie, G. Ventura, A review of extended/generalized finite element methods for material modeling, Model. Simul. Mater. Sci. Eng. 17 (2009) 1–24.
[3] I. Babuška, U. Banerjee, Stable generalized finite element method (SGFEM), Comput. Methods Appl. Mech. Eng. 201 (2012) 91–111.
[4] L. Berger-Vergiat, H. Waisman, B. Hiriyur, R. Tuminaro, D. Keyes, Inexact Schwarz-algebraic multigrid preconditioners for crack problems modeled by extended finite element methods, Int. J. Numer. Methods Eng. 90 (2012) 311–328.
[5] I. Babuška, U. Banerjee, K. Kergrene, Strongly stable generalized finite element method: application to interface problems, Comput. Methods Appl. Mech. Eng. 327 (2017) 58–92.
[6] X.-C. Cai, Y. Saad, Overlapping domain decomposition algorithms for general sparse matrices, Numer. Linear Algebra Appl. 3 (3) (1996) 221–237.
[7] X.-C. Cai, M. Sarkis, A restricted additive Schwarz preconditioner for general sparse linear systems, SIAM J. Sci. Comput. 21 (2) (1999) 792–797.
[8] C. Lang, D. Makhija, A. Doostan, K. Maute, A simple and efficient preconditioning scheme for heaviside enriched XFEM, Comput. Mech. 54 (5) (2014) 1357–1374.

[9] P. Fischer, Projection techniques for iterative solution of with successive right-hand sides, Comput. Methods Appl. Mech. Eng. 163 (1) (1998) 193–204.
[10] A. Frommer, D.B. Szyld, An algebraic convergence theory for restricted additive schwarz methods using weighted max norms, SIAM J. Numer. Anal. 39 (2) (2001) 463–479.
[11] B. Krank, N. Fehn, W. Wall, M. Kronbichler, A high-order semi-explicit discontinuous Galerkin solver for 3D incompressible flow with application to DNS and LES of turbulent channel flow, J. Comput. Phys. 348 (1) (2017) 634–659.
[12] N. Moes, J. Dolbow, T. Belytschko, A finite element method for crack growth without remeshing, Int. J. Numer. Methods Eng. 46 (1999) 131–150.
[13] A. Menk, S.P.A. Bordas, A robust preconditioning technique for the extended finite element method, Int. J. Numer. Methods Eng. 85 (2011) 1609–1632.
[14] P. Grisvard, Elliptic Problems in Nonsmooth Domains, Pitman Publishing, Inc, Boston, USA, 1985.
[15] V. Gupta, C.A. Duarte, I. Babuška, U. Banerjee, A stable and optimally convergent generalized FEM (SGFEM) for linear elastic fracture mechanics, Comput. Methods Appl. Mech. Eng. 266 (2013) 23–39.
[16] A. Gerstenberger, R. Tuminaro, Algebraic multigrid techniques for the extended finite element method, in: Copper Mountain Conference on Multigrid Methods, 2011.
[17] Y. Saad, Iterative Methods for Sparse Linear Systems, Society for Industrial and Applied Mathematics, Philadelphia, PA, USA, 2000.
[18] R. Tian, L. Wen, L. Wang, Three-dimensional improved XFEM (IXFEM) for static crack problems, Comput. Methods Appl. Mech. Eng. 343 (1) (2019) 339–367.
[19] H. Waisman, L. Berger-Vergiat, An adaptive domain decomposition preconditioner for crack propagation problems modeled by XFEM, Int. J. Multiscale Comput. Eng. 11 (6) (2013) 633–654.
[20] L. Wang, L. Wen, J. Wang, R. Tian, Implementations of parallel software for crack analyses based on the improved XFEM, Sci. Sin. Technol. 48 (11) (2018) 1241–1258.
[21] Q. Zhang, I. Babuška, U. Banerjee, Robustness in stable generalized finite element methods (SGFEM) applied to Poisson problems with crack singularities, Comput. Methods Appl. Mech. Eng. 311 (2016) 476–502.
[22] Q. Zhang, I. Babuška, A stable generalized finite element method (SGFEM) of degree two for interface problems, Comput. Methods Appl. Mech. Eng. 363 (1) (2020) 112889.
[23] F. Erdogan, G.C. Sih, On the crack extension in plate under plane loading and transverse shear, ASME J. Basic Eng. 85 (1963) 519–527.
[24] J.G. Williams, P.D. Ewing, Fracture under complex stress, the angled crack problem, Int. J. Fract. 26 (1984) 346–351.
[25] M. Gosz, J. Dolbow, B. Moran, Domain integral formulation for stress intensity factor computation along curved three dimensional interface cracks, Int. J. Solids Struct. 35 (15) (1998) 1763–1783.
[26] S. Loehnert, D.S. Mueller-Hoeppe, P. Wriggers, 3D corrected XFEM approach and extension to finite deformation theory, Int. J. Numer. Methods Eng. 86 (2011) 431–452.
[27] N. Moes, A. Gravouil, T. Belytschko, Non-planar 3D crack growth by the extended finite element and level sets-Part I: Mechanical model, Int. J. Numer. Methods Eng. 53 (2002) 2549–2568.
[28] M.L. Parks, E. de Sturler, G. Mackey, Recycling Krylov subspaces for sequences of linear systems, SIAM J. Sci. Comput. 28 (5) (2006) 1–26.
[29] H. Waisman, L. Berger-Vergiat, An adaptive domain decomposition preconditioner for crack propagation problems modeled by XFEM, Int. J. Multiscale Comput. Eng. 11 (6) (2013) 633–654.
[30] X. Chen, X.-C. Cai, An effective Schwarz preconditioner for crack problems modeled by extended finite element method, Commun. Comput. Phys. 28 (4) (2020) 1561–1584.